A modified plane channel code for flow with a spatially varying pressure gradient

A. Pinelli and M. Uhlmann
School of Aeronautics, U. Politécnica Madrid, Spain

October 19, 1999

1 Introduction

Our objective is to simulate turbulent wall-bounded shear flow undergoing an adverse pressure gradient. While this is clearly a configuration requiring an inflow/outflow method with all the corresponding problems in supplying the appropriate boundary conditions, we opt herein for a severe simplification of the numerical task. We maintain the streamwise periodicity of the flow as in classical channel flow computations and impose a non-linear pressure perturbation by an appropriate (mass-neutral) wall-transpiration. As a consequence, the flow undergoes positive and negative pressure perturbations to the driving pressure gradient successively at each passage through the domain. The zone of interest will therefore be of limited spatial extent according to the local pressure gradient and a "contamination" due to periodicity (history effects) cannot be excluded *a priori*.

We are interested in the wall-region which is free of the direct influence of transpiration (cf. [1]) and we will therefore consider the boundary layer opposite of the permeable surface. In this case it seems judicious to suppose the latter boundary to be a slip-surface which makes it less sensitive to flow separation. We expect to be able to reach higher pressure gradients within the "useful" boundary layer.

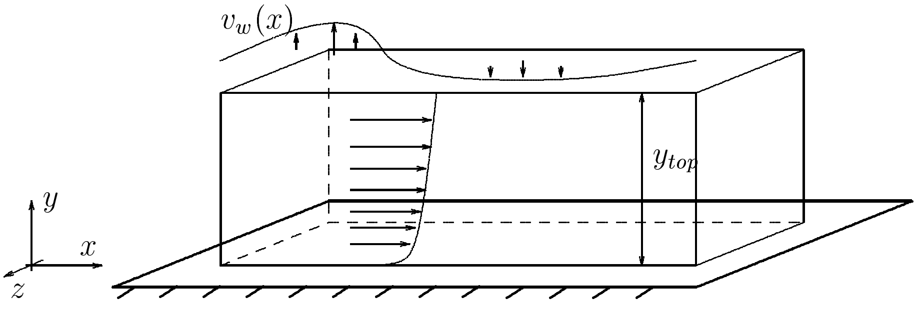

Figure 1: Coordinate system and computational domain of the modified channel flow simulations.

2 Modifications to the basic channel code

The physical boundary conditions at the extrema of the non-periodic direction y are the following (cf. figure 1 for a schematic of the domain):

$$\begin{array}{lll} \partial_y u = \partial_y w = 0\,, \quad v = v_w(x) & (y = y_{top}) & \\ u = v = w = 0 & (y = 0) & . \end{array} \tag{1}$$

At the lower wall the no-slip/impermeability condition leads to the usual condition

$$\partial_y u = \omega_y = v = 0 \qquad (y = 0) \quad , \tag{2}$$

which is more appropriate given our use of $\varphi = \nabla^2 v$ and ω_y as the evolution variables [1]. At the slip/permeable wall we get from continuity written in Fourier space:

$$\left.\begin{array}{lcl} i\,\alpha\,\partial_y \hat{u} + \partial_{yy}\hat{v} + i\,\beta\,\partial_y \hat{w} & = & 0 \\ \longrightarrow \partial_{yy}\hat{v} & = & 0 \end{array}\right\} \quad (y = y_{top}) \quad . \tag{3}$$

Therefor the Laplacian reads:

$$\hat{\varphi} = -(\alpha^2 + \beta^2)\,\hat{v}_w \qquad (y = y_{top}) \quad . \tag{4}$$

The gradient of the wall-normal vorticity reduces to

$$\partial_y \hat{\omega}_y = i\,\beta\,\partial_y \hat{u} - i\,\alpha\,\partial_y \hat{w} = 0 \qquad (y = y_{top}) \quad . \tag{5}$$

Consequently the Helmholtz problems for $\hat{\omega}_y$ have now a Dirichlet condition at the lower wall and a Neumann condition at the upper surface. The Galerkin treatment is now handled in the code by passing the flag "3" to the module `HELMHOLTZYL`. The bi-harmonic problem of φ and v is solved in the following way (the module `BIODDD`), adopting the notation of [1]:

$$\hat{v}^{n+k/3} = \hat{v}_p + c_1 \cdot \hat{v}_h \quad , \tag{6}$$

and consequently

$$\hat{\varphi}^{n+k/3} = \hat{\varphi}_p + c_1 \cdot \hat{\varphi}_h \quad , \tag{7}$$

where the particular $\{\hat{\varphi}_p, \hat{v}_p\}$ and homogeneous $\{\hat{\varphi}_h, \hat{v}_h\}$ parts are solutions of the following set of Helmholtz problems subject to homogeneous and non-homogeneous Dirichlet conditions:

$$\left.\begin{array}{lcl} \left[\mathbf{K} - (k_x^2 + k_z^2 + \dfrac{\mathrm{Re}}{\alpha_k \Delta t})\,\mathbf{M}\right] \cdot \hat{\boldsymbol{\varphi}}_p & = & \left[-\dfrac{\mathrm{Re}}{\alpha_k \Delta t}\,\mathbf{M}\right] \cdot \hat{\boldsymbol{\varphi}}^n - [\mathrm{Re}\,\mathbf{M}] \cdot \hat{\boldsymbol{h}}_v^{n+(k-1)/3} \\ \left[\mathbf{K} - (k_x^2 + k_z^2)\,\mathbf{M}\right] \cdot \hat{\boldsymbol{v}}_p & = & \mathbf{M} \cdot \hat{\boldsymbol{\varphi}}^{n+(k-1)/3} \\ \underline{\text{with}}: \quad \hat{\varphi}_p(y=0) = 0\,, & & \hat{\varphi}_p(y=y_{top}) = -(\alpha^2 + \beta^2)\,\hat{v}_w\,, \\ \hat{v}_p(y=0) = 0\,, & & \hat{v}_p(y=y_{yop}) = \hat{v}_w \end{array}\right\} \tag{8}$$

$$\left.\begin{array}{lcl} \left[\mathbf{K} - (k_x^2 + k_z^2 + \dfrac{\mathrm{Re}}{\alpha_k \Delta t})\,\mathbf{M}\right] \cdot \hat{\boldsymbol{\varphi}}_{h1} & = & 0 \\ \left[\mathbf{K} - (k_x^2 + k_z^2)\,\mathbf{M}\right] \cdot \hat{\boldsymbol{v}}_{h1} & = & \mathbf{M} \cdot \hat{\boldsymbol{\varphi}}^{n+(k-1)/3} \\ \underline{\text{with}}: \quad \hat{\varphi}_{h1}(y=0) = 1\,, & & \hat{\varphi}_{h1}(y=y_{top}) = 0\,, \\ \hat{v}_{h1}(y=0) = 0\,, & & \hat{v}_{h1}(y=y_{top}) = 0 \end{array}\right\} \tag{9}$$

The constant coefficient c_1 is determined such that the homogeneous Neumann condition on v is satisfied on the lower wall by the final solution, viz:

$$c_1 = -\frac{\partial_y \hat{v}_p(0)}{\partial_y \hat{v}_h(0)} \tag{10}$$

The final solution $\{\hat{v}^{n+k/3}, \hat{\varphi}^{n+k/3}\}$ can then be calculated from relations (6) and (7).

Although the pressure is not needed explicitly for advancing the computation in time, we wish to reconstruct it as a result. Therefore, it is sufficient to perform the reconstruction only as frequent as the update of the usual statistics, i.e. every `ISTATI` steps. The appropriate boundary conditions for pressure can be derived from the momentum equations. Writing the x-component at $y=0$ gives:

$$\underbrace{\partial_t u}_{=0} + \underbrace{u \cdot \partial_x u + v \cdot \partial_y u + w \cdot \partial_z u}_{=0} + \partial_x p = \frac{1}{\mathrm{Re}} \nabla^2 u \qquad (y=0)$$

$$\longrightarrow \hat{p} = -i \, \frac{1}{Re\,\alpha} \, \partial_{yy} \hat{u} = \frac{i}{Re\,\alpha} \partial_y \hat{\omega}_z \qquad (\alpha \neq 0, y=0) \quad . \tag{11}$$

Similarly, the z-momentum gives:

$$\hat{p} = -i \, \frac{1}{Re\,\beta} \, \partial_{yy} \hat{w} = \frac{i}{Re\,\beta} \partial_y \hat{\omega}_x \qquad (\beta \neq 0, y=0) \quad , \tag{12}$$

while

$$\hat{p} = 0 \qquad \forall \quad y \qquad (\alpha = 0, \beta = 0) \quad . \tag{13}$$

At the upper boundary, we use first the y-derivative of streamwise momentum, viz:

$$\underbrace{\partial_t \partial_y u}_{=0} + \underbrace{\partial_y u}_{=0} \cdot \partial_x u + u \cdot \underbrace{\partial_{yx} u}_{=0} + \partial_y v \cdot \underbrace{\partial_y u}_{=0} + v \cdot \partial_{yy} u + \underbrace{\partial_y w}_{=0} \cdot \partial_z u + w \cdot \underbrace{\partial_{yz} u}_{=0} + \partial_{yx} p = \frac{1}{\mathrm{Re}} \nabla^2 \partial_y u$$

$$\longrightarrow \partial_y \hat{p} = -i \, \frac{1}{\alpha} \left(\frac{1}{Re} \partial_{yyy} \hat{u} - \widehat{v \partial_{yy} u} \right) \qquad (\alpha \neq 0, y = y_{top}) \quad . \tag{14}$$

Similarly from the z-derivative of wall-normal momentum:

$$\underbrace{\partial_t \partial_z v}_{=0} + \partial_z u \cdot \partial_x v + u \cdot \underbrace{\partial_{zx} v}_{=0} + \underbrace{\partial_z v}_{=0} \cdot \partial_y v + v \cdot \partial_{yz} v + \partial_z w \cdot \underbrace{\partial_z v}_{=0} + w \cdot \underbrace{\partial_{zz} v}_{=0} + \partial_{yz} p = \frac{1}{\mathrm{Re}} \nabla^2 \partial_z v$$

$$\longrightarrow \partial_y \hat{p} = \frac{1}{Re} \hat{\varphi} + \frac{i}{\beta} \left(\widehat{\partial_z u \partial_x v} + \widehat{v \partial_{yz} v} \right) \qquad (\beta \neq 0, y = y_{top}) \quad . \tag{15}$$

The above conditions necessitate again a superposition of particular and homogeneous solutions according to:

$$p^{n+k/3} = p_p + c_1 \cdot p_{h1} \quad , \tag{16}$$

where the respective contributions are obtained from the solution of the following Helmholtz problems:

$$\left. \begin{array}{lll} \left[\mathbf{K} - (k_x^2 + k_z^2) \mathbf{M} \right] \cdot \hat{\boldsymbol{p}}_p & = & -\mathbf{M} \cdot (\widehat{\partial_{x_i} \boldsymbol{H}})_i^{n+(k-1)/3} \\ \underline{\text{with}}: \quad \hat{p}_p(y=0) = \hat{p} \text{ from (11) and (12)}, & & \hat{p}_p(y=y_{top}) = 0 \end{array} \right\} \tag{17}$$

$$\left. \begin{array}{lll} \left[\mathbf{K} - (k_x^2 + k_z^2) \mathbf{M} \right] \cdot \hat{\boldsymbol{p}}_{h1} & = & 0 \\ \underline{\text{with}}: \quad \hat{p}_{h1}(y=0) = 0\,, & & \hat{p}_{h1}(y=2h) = 1 \end{array} \right\} \tag{18}$$

The coefficient c_1 is then obtained from the following relation:

$$c_1 = \frac{b - \partial_y p_p(y_{top})}{\partial_y p_{h1}(y_{top})}, \qquad \text{where } b{=}\partial_y \hat{p} \text{ from (14) and (15)} \quad . \tag{19}$$

The advantage of this particular way of solving the Helmholtz problem lies in the fact that we impose the boundary pulse to the homogeneous solution at the same extremum where we evaluate the derivative. Therefore, no problems with stiffness of the involved exponentials are encountered.

The described changes to the pressure algorithm affect the module `CALPRES` and the ones called by it. Several supplementary modifications were necessary for calculating the boundary conditions: (i) storage of the vorticities needed for (11) and (12) in the (x, z, y_{top})-plane performed in module `CALCVORTWALL` called from `SOLVOR`; (ii) utilities for performing two-dimensional FFT's and derivatives in the (x, z, y_{top})-plane only since the non-linear conditions (14) and (15) need to be evaluated pseudo-spectrally $\rightarrow$ modules `FOURXZ2D` and `DERIV2D`; (iii) calculation of second and third derivative at the extrema of a wall-normal data column, involving the collocation finite-difference formula and the derivatives of the mapping function (cf. §2.1). The actual assembly of the non-linear conditions (14) and (15) is performed in two steps in modules `CALUTERMA` (called from `SOLUV`) and `CALUTERMB` (called from `DELTSTP`); in between, the data "strips" – cut in the spanwise direction – from the first step are gathered by the last processor (subroutine `BCASTUTERM`) in order to be able to perform FFT's in the (x, z, y_{top})-plane.

2.1 Explicit higher order derivative formulas for the end-points of the domain

We define a one-sided stencil as follows

$$\begin{aligned} s_1'' &= \frac{1}{h^2} \sum_{l=1}^{8} c_l'' \cdot f(\xi_l) \\ s_1''' &= \frac{1}{h^3} \sum_{l=1}^{8} c_l''' \cdot f(\xi_l) \quad . \end{aligned} \tag{20}$$

The collocation points ξ_l in the *equidistant* coordinate are (cf. [1]):

$$\xi_l = \{0, \frac{1}{2}h, \frac{3}{4}h, h, 2h, \ldots, L_y - h, L_y - \frac{3}{4}h, L_y - \frac{1}{2}h, L_y\} \quad , \tag{21}$$

where $h = L_y/(N_s - 5)$ is the equidistant mesh spacing for N_s collocation points. The coefficients and the respective truncation errors

$$\begin{aligned} s_j'' &= f_1'' + \alpha f_j^{viii} h^6 + \mathcal{O}(h^7) \\ s_j''' &= f_1''' + \alpha f_j^{vii} h^4 + \mathcal{O}(h^5) \quad , \end{aligned}$$

are given in the table 2.1. We note that the sign of the coefficients c_l''' is inverted at the other boundary of the domain. The coefficients are stored in the include-file `BLOCKNEW`.

Recalling that we use an analytical grid mapping $g(\xi) \rightarrow y$, viz

$$g(\xi) = 1 + \frac{\tanh(2\alpha(\xi - 1)\pi)}{\tanh(2\alpha\pi)} \qquad 0 \leq \xi \leq 2 \quad , \tag{22}$$

we then evaluate wall-normal derivatives according to the following compound formulas:

$$\begin{aligned} \frac{\partial \phi(y)}{\partial y} &= \frac{\partial \phi(y)}{\partial \xi} \cdot \frac{\partial \xi}{\partial y} \\ \frac{\partial^2 \phi(y)}{\partial y^2} &= \frac{\partial^2 \phi(y)}{\partial \xi^2} \cdot \left(\frac{\partial \xi}{\partial y}\right)^2 + \frac{\partial \phi(y)}{\partial \xi} \cdot \frac{\partial^2 \xi}{\partial y^2} \\ \frac{\partial^2 \phi(y)}{\partial y^2} &= \frac{\partial^3 \phi(y)}{\partial \xi^3} \cdot \left(\frac{\partial \xi}{\partial y}\right)^3 + 3\,\frac{\partial^2 \phi(y)}{\partial \xi^2} \cdot \frac{\partial \xi}{\partial y} \cdot \frac{\partial^2 \xi}{\partial y^2} + \frac{\partial \phi(y)}{\partial \xi} \cdot \frac{\partial^3 \xi}{\partial y^3} \quad . \end{aligned} \tag{23}$$

derivative	c_1	c_2	c_3	c_4	c_5	c_6	c_7	c_8	α
2nd	$\frac{875}{36}$	$-\frac{7936}{45}$	$\frac{8421376}{29835}$	$-\frac{277}{2}$	$\frac{307}{30}$	$-\frac{317}{135}$	$\frac{23}{52}$	$-\frac{13}{306}$	$-\frac{337}{26880}$
3rd	-65	$\frac{3904}{7}$	$-\frac{12288}{13}$	479	-31	5	$-\frac{44}{91}$	0	$-\frac{797}{6720}$

Table 1: Coefficients of explicit finite difference formulas for second and third derivatives at the extrema of the wall-normal direction of the domain.

This procedure involves storing first, second and third derivatives of the mapping function during initialization of the code (module `MAPDY`). The actual end-point derivatives are computed by calls to the subroutine `DERYEND23`.

The shape of the mapping (22) is symmetric with respect to the point $y = y_{top}/2$, which does not seem adequate for the present problem. However, we need to assure a significant resolution near the top boundary for the accuracy of our implemented Neumann boundary conditions. This conditions stems from the hybrid Galerkin/collocation character of our method.

3 Preliminary results from a case without transpiration

We have performed a first simulation with the present code where the top boundary is impermeable, i.e. $v_w(x) = 0$. The outer flow Reynolds number is $Re = U_0\, y_{top}/(2\,\nu) = 3250$, leading to a friction Reynolds number $Re_\tau = u_\tau\, y_{top}/(2\,\nu) = 174$. The extent of the domain is $L_x/(y_{top}/2) = 2\,\pi/2.34$ in the streamwise and $L_z/(y_{top}/2) = 2\,\pi/3.96$ in the spanwise direction. We used $N_x = 128$, $N_y = 160$ and $N_z = 96$ collocation points (before dealising).

Figure 6 shows the temporal evolution of the plane averaged shear stress (skin friction) of the present simulation which has been started from a doubly no-slip/impermeable case, setting the mean velocity to a half-channel profile at the initialization and filtering all perturbations by a tanh filter above $y = y_{top}/2$. The statistics have been accumulated after an initial transient of $t\,U_0/(y_{top}/2) \approx 25$.

Figure 5 indicates the state of convergence of the accumulated statistics.

Figures 2-4 show the one-point first and second-order statistics of the present case. Also included for comparison are the reference curves of the simulation with two “normal” no-slip/-impermeable walls, termed “case I1”. We note that the top-wall boundary condition seems to perturb the statistics only quite locally. Near the lower wall, discrepancies with respect to the reference case are probably due to the limited statistical sample of the present case.

Figure 7 shows snapshots of the reconstructed pressure field during the simulation.

4 Outlook

As a next step, an appropriate shape of the upper wall-transpiration $v_w(x)$ needs to be selected and tested. Furthermore, an appropriate accumulation of two-dimensional statistics within the code should be implemented. The calculation of the streamwise evolution of shape factor etc. could be done by a post-processor very similar to the one in `gongora:/home1/uhlmann/EXTRACT/-extrau00/extrauxy.f`.

References

[1] J. Jiménez, A. Pinelli, and M. Uhlmann. Plane channel flow simulation over porous walls. Technical Note ETSIA MF-9809, School of Aeronautics, Universidad Politécnica Madrid, Spain, 1998.

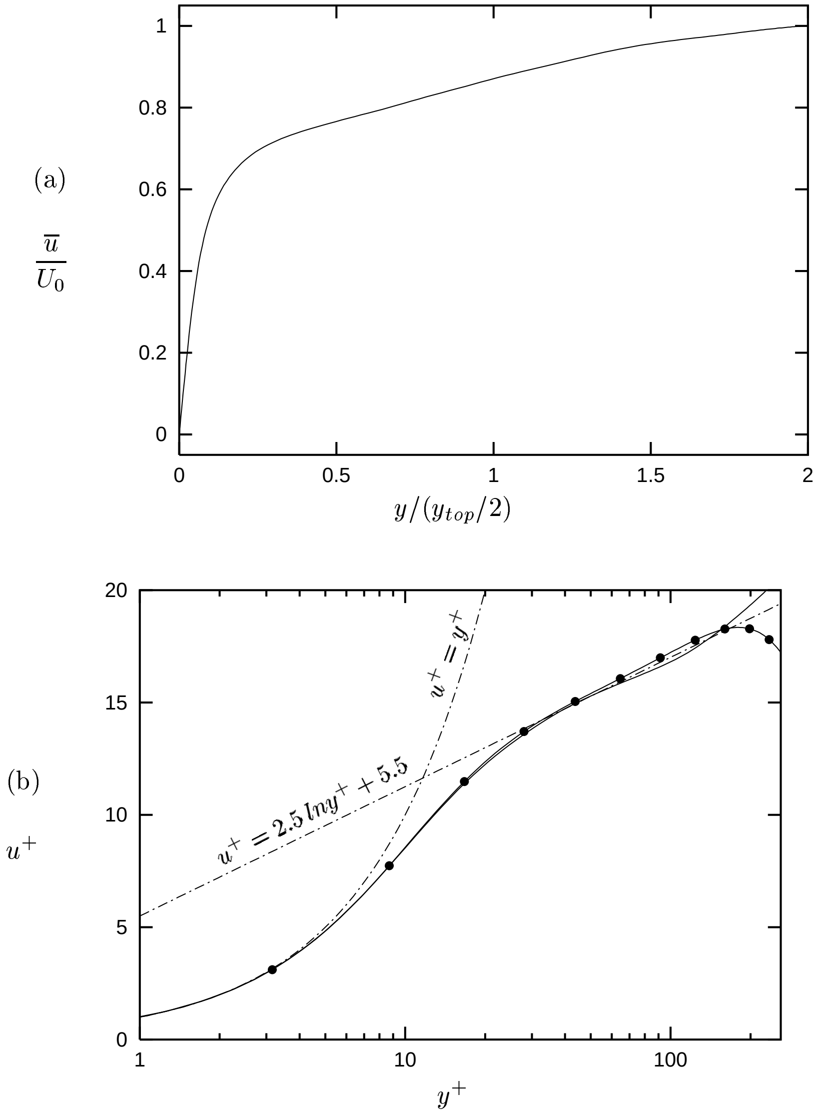

Figure 2: Mean velocity profiles of the present case and case I1 (lines with symbols) in (a) global coordinates and (b) wall-coordinates.

(a)

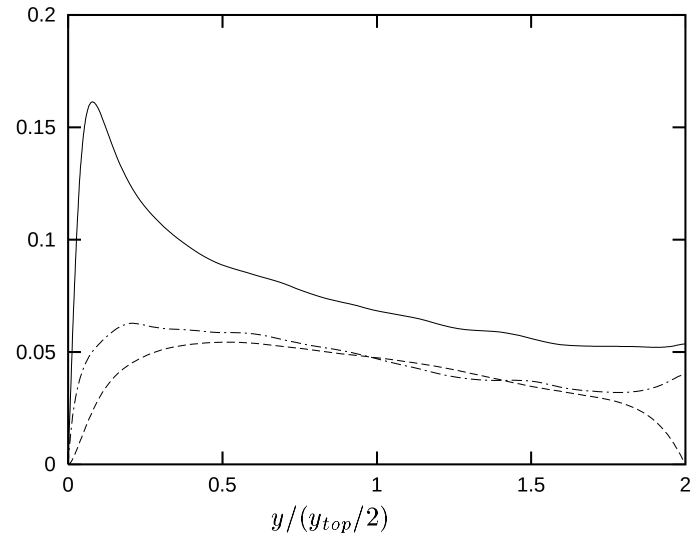

(b)

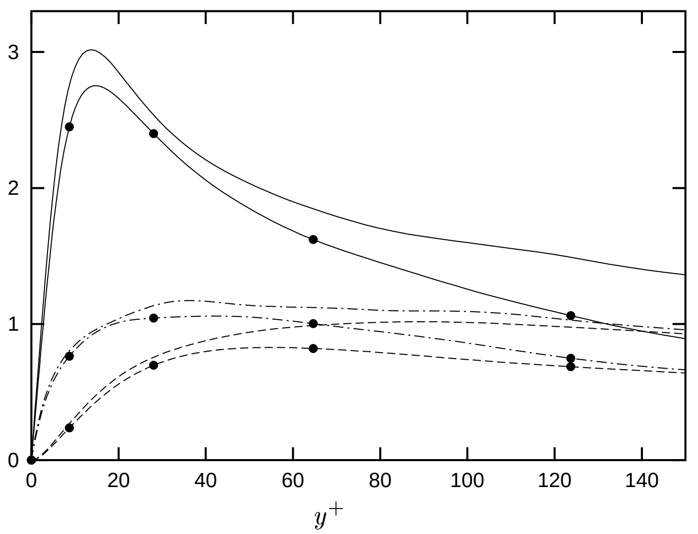

Figure 3: Root-mean-square velocity profiles of the present case and case I1 (lines with symbols) in (a) global coordinates and (b) wall-coordinates. ——— , u; - - - - , v; —·— , w.

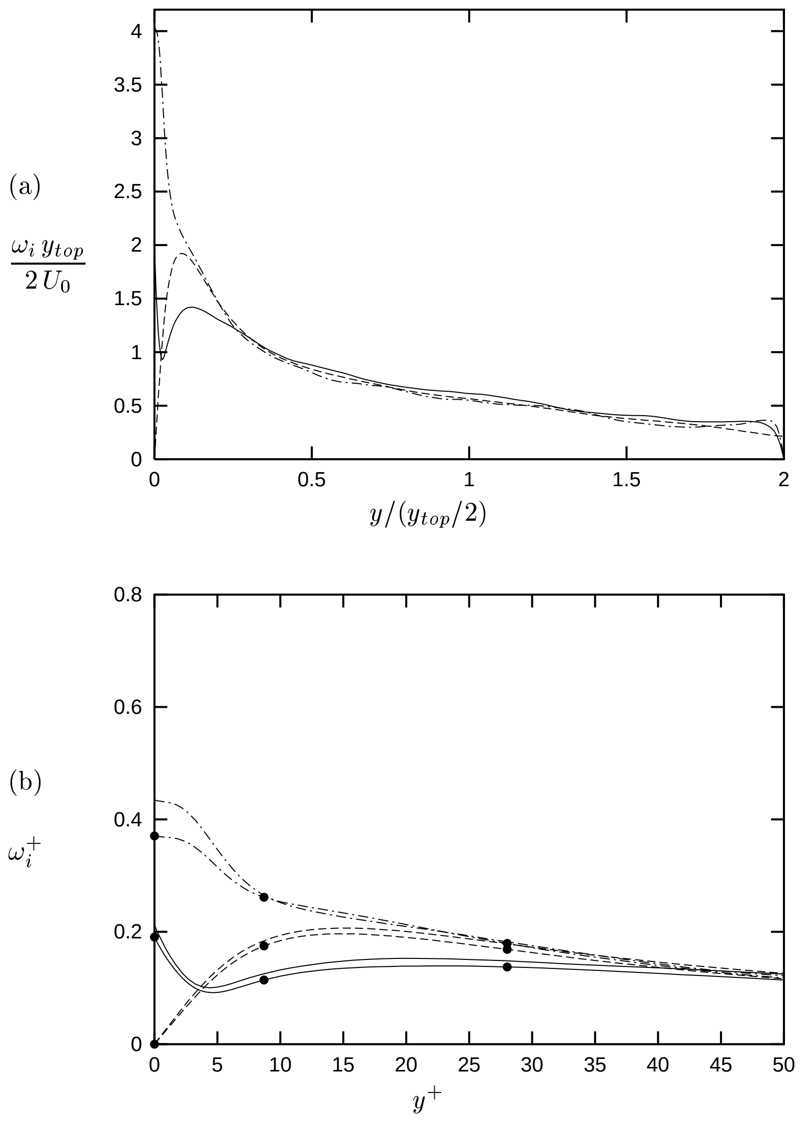

Figure 4: Root-mean-square vorticity profiles of the present case and case P2 (lines with symbols) in (a) global coordinates and (b) wall-coordinates. ——— , ω_x; - - - - , ω_y; —·— , ω_z.

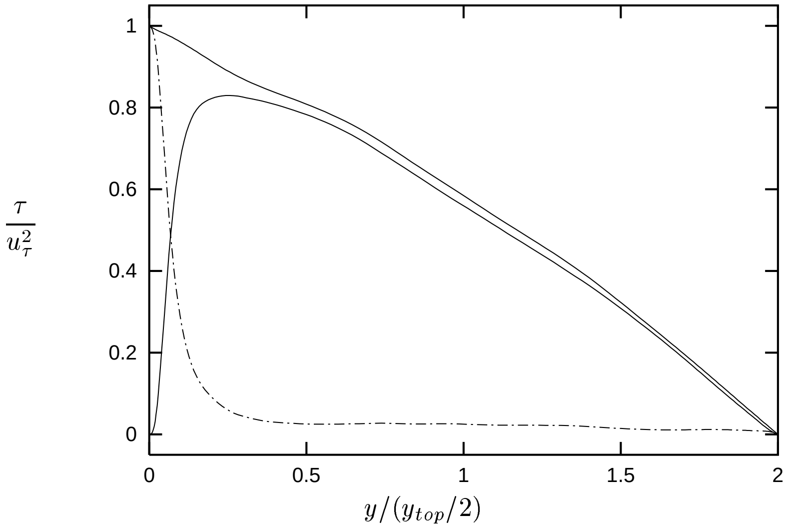

Figure 5: Profiles of the shear-stress contributions: ——— , total stress; - - - - , $-\nu\,\partial_y\,\overline{u}$; —·— , $\overline{u'v'}$.

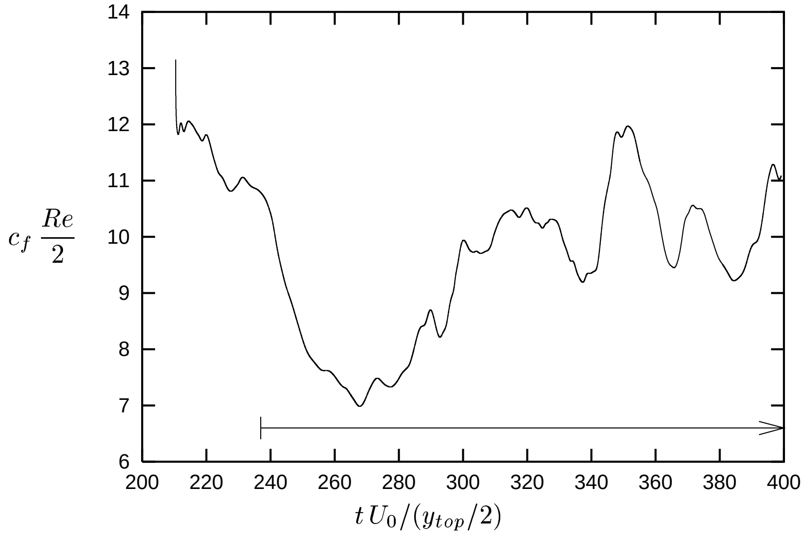

Figure 6: Evolution of the plane-averaged wall-friction of the present case. The arrow indicates the time span of accumulation of statistics.

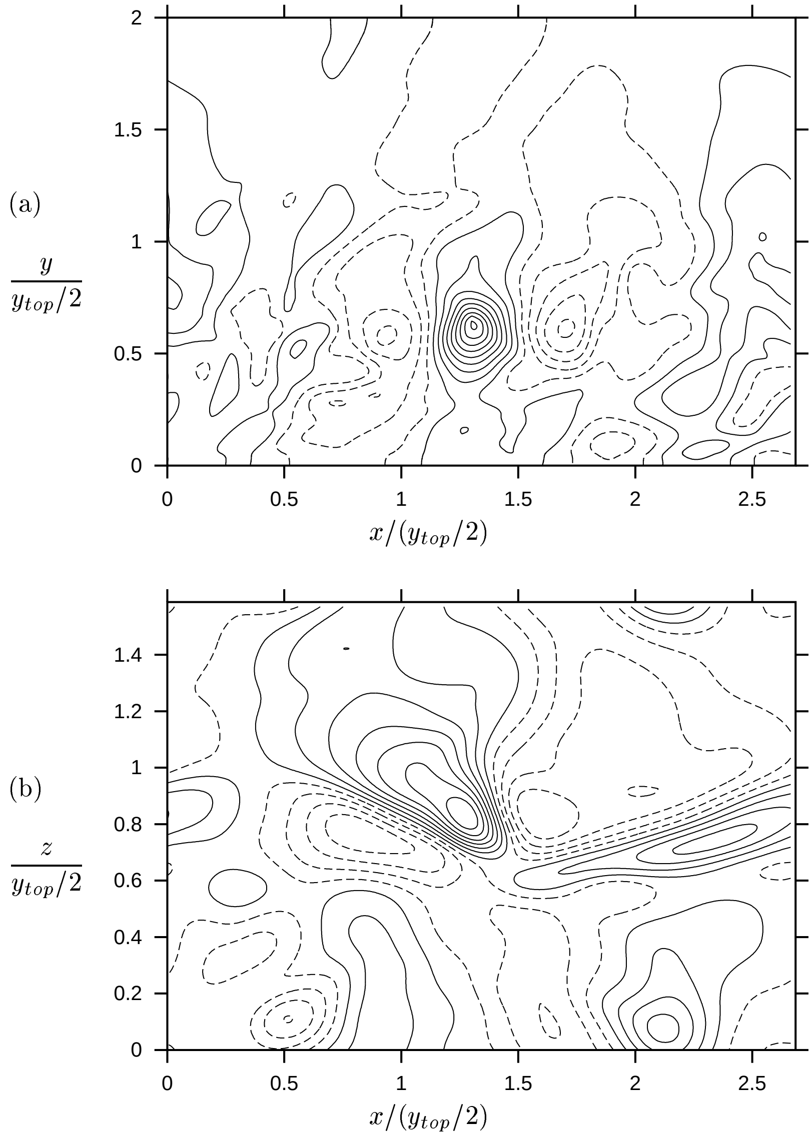

Figure 7: Instantaneous contours of pressure perturbation. (a) the $(k_z = 0)$-mode, $p'/(U_0^2\rho) = -0.0085\,(.001) + 0.0045$; (b) the $(y = 0)$-plane, $p'/(U_0^2\rho) = -0.02\,(.003) + 0.01$. Negative values are dashed.